Published in IET Power Electronics
Received on 1st August 2011
Revised on 28th December 2011
doi: 10.1049/iet-pel.2011.0300

ISSN 1755-4535

Hysteresis current control of hybrid active power filters

C.-S. Lam[1] *M.-C. Wong*[1] *Y.-D. Han*[1,2]

[1]*Department of Electrical and Computer Engineering, University of Macau, Macao, People's Republic of China*
[2]*Department of Electrical Engineering, Tsinghua University, Beijing, People's Republic of China*
E-mail: cslam@umac.mo; C.S.Lam@ieee.org

Abstract: This article presents a hysteresis pulse width modulation study for a inductor-capacitor (LC)-coupling hybrid active power filter (HAPF). As the coupling LC impedance yields a non-linear inverter current slope, this can affect the controllability of using the conventional hysteresis control method and generate unexpected trigger signals to the switching devices. This results in deteriorating the system operating performances. On the basis of the proposed modelling, the linearisation of the hysteresis control for the HAPF is firstly studied, investigated and compared with the linear active power filter. Two limits are proposed in this study that divides the HAPF into non-linear, quasi-linear and linear operation regions. The design criteria of hysteresis band and sampling time can then be derived. Single-phase simulation and experimental results are given to verify the hysteresis control study of HAPF compared with active power filter. Finally, representative simulation and experimental results of a three-phase four-wire centre-split HAPF for power quality compensation are presented to demonstrate the validity of the hysteresis linearisation study.

1 Introduction

Pulse width modulation (PWM) techniques such as hysteresis, ramp comparison and space vector were traditionally developed based on linear concept [1]. They are usually applied on the conventional linear *L*-coupling voltage source inverters for different applications [1–9], such as ac motor drives, active power filter (APF) and dynamic voltage restorer. Among different PWM methods, hysteresis is one of the most popular PWM strategies [2–5] and widely applied in APF for current quality compensation, owing to its advantages such as ease of implementation, fast dynamic response and current limiting capability. However, the initial and operational costs of APF are high [10–12], thus slows down its large-scale application in distribution power networks. To overcome this problem, a transformerless LC-coupling hybrid active power filter (HAPF) has been recently proposed and applied for current quality compensation and damping of harmonic propagation in distribution power systems [13–16], in which it contains less passive components and the dc-link operating voltage can be much lower than the APF, thus reducing the system cost. Its low dc-link voltage characteristic is due to the system fundamental voltage dropped across the coupling capacitance but not the inverter part of the HAPF [14].

In recent research studies, the design principles and filtering characteristics for the LC-coupling HAPF have been presented and discussed [13]. An optimal design of its dc-link voltage has been introduced based on the vector trajectory method [14]. In order to enhance the LC-coupling HAPF system response, a novel control technique has also been proposed [15]. As the coupling LC yields a non-linear inverter current slope, this can affect the controllability of using the conventional hysteresis control method and generate unexpected trigger signals to the switching devices, thus deteriorating the system operating performances. However, there is still no research work examining nor discussing the minimum operating requirement for this HAPF (i.e. LC-coupling voltage source inverter) if the linear hysteresis control strategy is applied.

In this study, the modelling of the LC-coupling HAPF will be firstly presented. Via its modelling, the linearisation work of hysteresis control for this HAPF will be studied in comparison to the linear APF. Two limits quasi-linear limit and linear limit which divide the HAPF into non-linear, quasi-linear and linear operation regions are proposed. With respect to different LC values, this study aims to define the corresponding requirements for hysteresis band and sampling time, such that the inverter current slope of the HAPF can be treated as linear using the hysteresis method. Otherwise, unexpected trigger signals will be generated to the switching devices and strongly affect the HAPF compensating performances. Finally, simulation and experimental results for single-phase and three-phase systems are presented to verify the hysteresis control study for HAPF compared with that of linear APF.

2 Modelling of a two-level three-phase four-wire centre-split HAPF and APF

2.1 Circuit configuration of a two-level three-phase four-wire centre-split HAPF and APF

Fig. 1 illustrates the circuit configuration of a two-level three-phase four-wire HAPF and APF, where the subscript '*x*' denotes phase *a*, *b*, *c*, *n*. v_{sx} is the system voltage, v_x is the load voltage, L_s is the system inductance normally

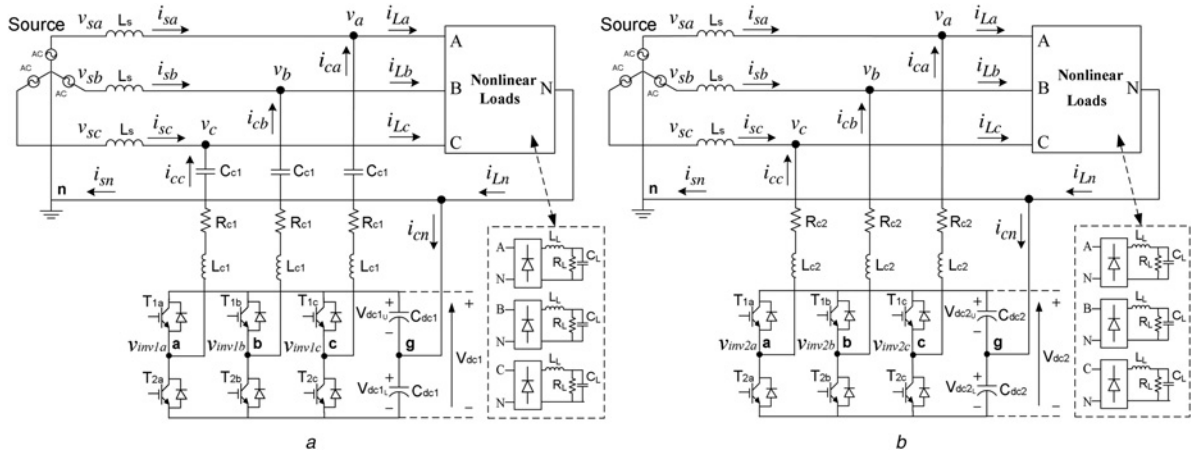

Fig. 1 *Circuit configuration of a two-level three-phase four-wire centre-split compensator*

a HAPF
b APF

neglected due to its low value relatively, thus $v_{sx} \simeq v_x$. i_{sx}, i_{Lx} and i_{cx} are the system, load and inverter current for each phase. C_{c1}, L_{c1} and R_{c1} are the coupling part capacitance, inductance and internal resistance of the HAPF, in which C_{c1} and L_{c1} are designed basing on the reactive power consumption and the dominant harmonic current of the inductive loading. L_{c2} and R_{c2} are the coupling part inductance and internal resistance of the APF, in which L_{c2} is designed basing on the switching frequency, switching ripple and dc-link voltage-level consideration. C_{dc1}, V_{dc1U} and V_{dc1L} are the dc capacitor, upper and lower dc capacitor voltages of the HAPF, while C_{dc2}, V_{dc2U} and V_{dc2L} are the dc capacitor, upper and lower dc capacitor voltages of the APF. The dc-link midpoint is assumed to be ground reference (g). From Fig. 1, the inverter line-to-ground voltages $v_{invjx-g}$ will be equal to the inverter line-to-neutral voltages $v_{invjx-n}$ because the neutral point n is connected with the dc-link midpoint g, where subscript $j = 1$ represents the HAPF and $j = 2$ represents the APF. The non-linear loads are composed of three single-phase diode bridge rectifiers, which act as harmonic producing loads in this study. In the following, all the analyses are based on sufficient dc-link voltage assumption.

2.2 Modelling of a two-level three-phase four-wire centre-split HAPF and APF

From Fig. 1, the switching functions S_x for each inverter leg of HAPF and APF can be given as

$$S_x = \begin{cases} 1 & \text{when } T_{1x} \text{ is ON and } T_{2x} \text{ is OFF} \\ -1 & \text{when } T_{2x} \text{ is ON and } T_{1x} \text{ is OFF} \end{cases} \quad (1)$$

For $V_{dcj_U} = V_{dcj_L} = 0.5\,V_{dcj}$, the output voltage for each inverter leg can be expressed as

$$v_{invjx} = S_x \times 0.5\,V_{dcj} \quad (2)$$

The inverter line-to-neutral voltage $v_{invjx-n}$ can be expressed as

$$v_{invjx-n} = v_{invjx} - v_n = v_{invjx} \quad (3)$$

where the neutral line voltage $v_n = 0$, the switching state of an inverter leg is independent of the switching states of the other two legs, the inverter line-to-neutral voltage $v_{invjx-n}$ for each leg is either equal to $-0.5V_{dcj}$ or $+0.5V_{dcj}$. From Fig. 1*a*, the relationship among the inverter current i_{cx}, load voltage v_x, coupling capacitor voltage v_{Cc1x} and inverter line-to-neutral voltage v_{inv1x} of the HAPF is

$$L_{c1}\frac{di_{cx}(t)}{dt} + R_{c1}i_{cx}(t) = v_{inv1x}(t) - v_x(t) - v_{Cc1x}(t) \quad (4)$$

From (2), the modelling for each inverter leg of the HAPF can be expressed as

$$L_{c1}\frac{di_{cx}(t)}{dt} + R_{c1}i_{cx}(t) = S_x \times 0.5\,V_{dc1} - v_x(t) - v_{Cc1x}(t) \quad (5)$$

$$C_{c1}\frac{dv_{Cc1x}(t)}{dt} = i_{cx}(t) \quad (6)$$

From Fig. 1*b*, the relationship among the inverter current i_{cx}, load voltage v_x and inverter line-to-neutral voltage v_{inv2x} of the APF is

$$L_{c2}\frac{di_{cx}(t)}{dt} + R_{c2}i_{cx}(t) = v_{inv2x}(t) - v_x(t) \quad (7)$$

From (2), the modelling for each inverter leg of the APF can be expressed as

$$L_{c2}\frac{di_{cx}(t)}{dt} + R_{c2}i_{cx}(t) = S_x \times 0.5\,V_{dc2} - v_x(t) \quad (8)$$

Via (4)–(8), the linearisation study of hysteresis control for the HAPF in comparison to the linear APF will be presented in the following.

3 Hysteresis PWM control for the HAPF

As the coupling LC of the HAPF yields a non-linear inverter current slope, this can affect the controllability of using the conventional hysteresis PWM, the linearisation of the hysteresis control for the HAPF should be investigated. In this study, the slope of the HAPF inverter current i_{cx} is categorised into three operation regions: (i) non-linear

doi: 10.1049/iet-pel.2011.0300

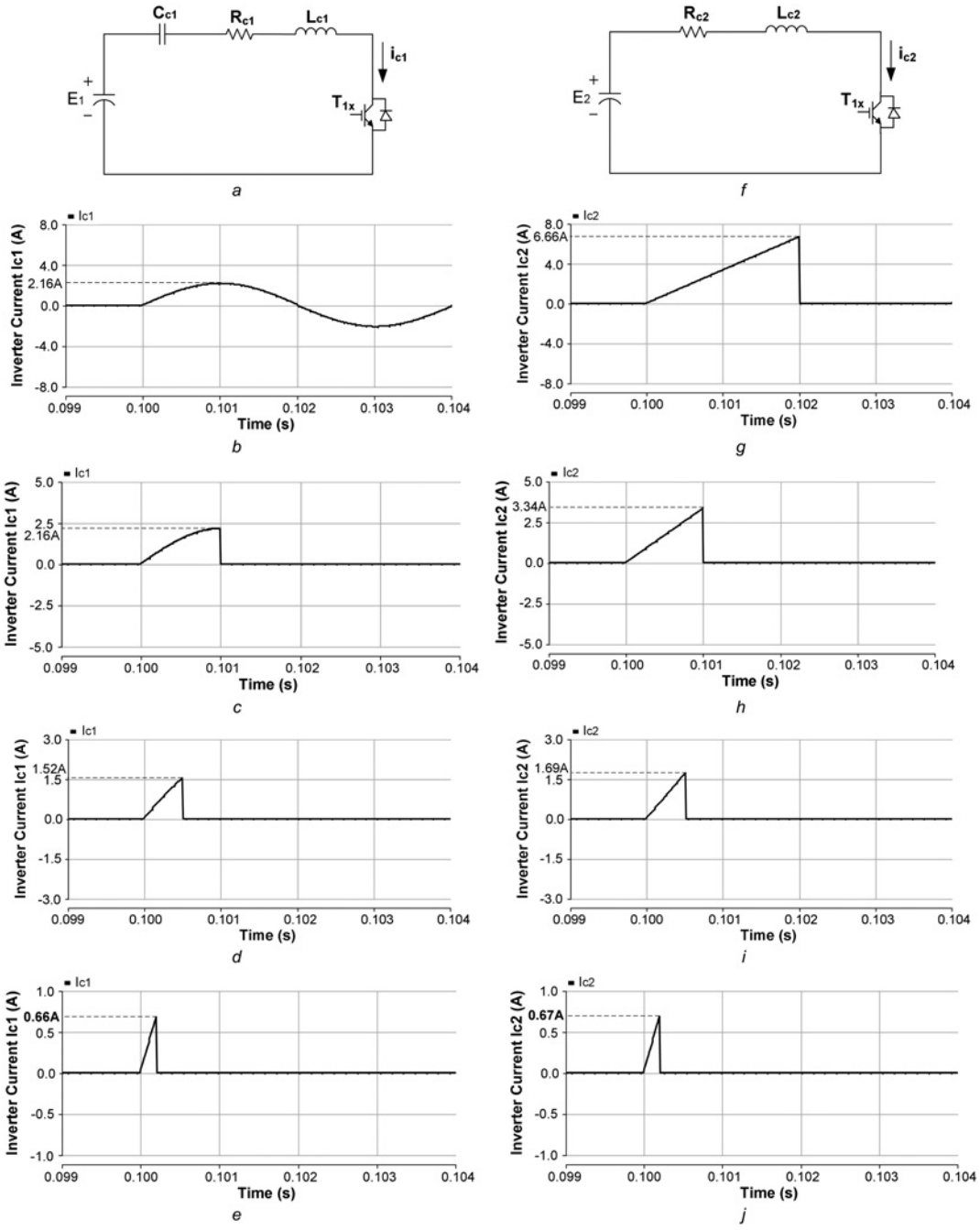

Fig. 2 *Simulated i_{c1} of HAPF and i_{c2} of APF single-phase model at different t_{on} interval and E_1, $E_2 = 20$ V*

HAPF:
a Single-phase model for T_{1x} at different t_{on} interval
b $t_{on} = 2000$ μs (non-linear)
c $t_{on} = 1000$ μs (quasi-linear)
d $t_{on} = 500$ μs (quasi-linear)
e $t_{on} = 200$ μs (linear)
APF:
f Single-phase model for T_{1x} at different t_{on} interval
g $t_{on} = 2000$ μs (linear)
h $t_{on} = 1000$ μs (linear)
i $t_{on} = 500$ μs (linear)
j $t_{on} = 200$ μs (linear)

region, (ii) quasi-linear region and (iii) linear region, in which their corresponding definitions and diagrams under hysteresis control are given in Appendix 8.1. In addition, these three operation regions are separated by two limits: quasi-linear limit T_{limit} and linear limit T_{linear}, in which their values are determined based on a constant reference inverter current i^*_{cx} assumption as given in Appendix 8.2. After that, the corresponding quasi-linear limit H_{limit} and linear limit H_{linear} for the hysteresis band can be obtained in Appendix 8.3. In the following, these three definitions and two limits will be used for the HAPF inverter current slope linearity justification under hysteresis control method.

In practical case, since different loading situations may require different coupling C_{c1} and L_{c1} values, thus yielding different T_{limit} (H_{limit}) and T_{linear} (H_{linear}) values (Appendix 8.1–8.3), it is important and necessary to carry out this linearity analysis, so that the linear operation region for each HAPF system can be achieved. In order to simplify the verification, the coupling part internal resistance for the HAPF and APF is approximately treated as zero ($R_{c1} \simeq 0$ and $R_{c2} \simeq 0$) in the following simulations and experiments because their values are usually small in practical situation.

3.1 Single-phase simulation and experimental results for HAPF inverter current slope linearisation analysis

Under constant reference inverter current i_{cx}^{*} assumption, Figs. 2*a* and *f* illustrate the HAPF and APF single-phase inverter current slope linearisation study models for upper switch T_{1x} at different switching on interval ($t = t_{on}$), in which the upper switch is an insulated gate bipolar transistor (IGBT). E_1 and E_2 represent the instantaneous peak voltage difference between the inverter output voltage and load voltage. Reversing the polarity of E_1 and E_2 will yield their models for lower switch T_{2x} ($t = t_{off}$). As the only difference between upper and lower switches is the opposite current polarity, the results for T_{2x} will not be included in this study. In short, E_1 and E_2 can be treated as dc voltage inputs. In addition, the load voltage is treated as a constant value for the following analysis. Table 1 lists the system parameters of HAPF and APF single-phase models. When $R_{c1} \simeq 0$ and $R_{c2} \simeq 0$, the current slope for APF will be linear no matter what the switching interval is, as verified by (7) and (8). As E_1 and E_2 values do not affect the determination results of the quasi-linear limit and linear limit, E_1 and E_2 are chosen as 20 V in this study. From Table 1, the quasi-linear limit and linear limit for HAPF will be $T_{limit} = 1000$ μs and $T_{linear} = 200$ μs, respectively. Simulation studies were carried out by using power system computer aided design (PSCAD)/electro magnetic transient in DC system (EMTDC). In the following, simulation and experimental results for Figs. 2*a* and *f* will be given to verify the HAPF inverter current slope linearisation analysis compared with the linear APF. Figs. 2 and 3 illustrate the simulated and experimental inverter current i_{c1} and i_{c2} for their single-phase models at different switching on interval.

In order to satisfy the linear region definition $|(\mathrm{d}i_{cx})/\mathrm{d}t|_{error} \leq 5\%$ (Appendix 8.1–8.2), the slope error of HAPF inverter current i_{c1} compared with the APF one i_{c2} should be less than 5%. From Fig. 2*b*, when $t_{on} > 1000$ μs, which is larger than the quasi-linear limit ($T_{limit} = 1000$ μs), the slope of i_{c1} as in Fig. 2*b* is non-linear compared with that of i_{c2} as shown in Fig. 2*g*. However, even when $t_{on} = 1000$ and 500 μs satisfy the quasi-linear limit, they do not satisfy the linear limit. It is obvious that Figs. 2*c*–*d* contain current slope errors (35.3%, 10.0%) compared with that of APF as shown in Figs. 2*h*–*i*. These errors have the potential of deteriorating the system operating performance significantly. When $t_{on} = 200$ μs, which satisfies the linear limit ($T_{linear} = 200$ μs), the current slope error decreases to 1.5% (within the linear region definition $|(\mathrm{d}i_{cx})/\mathrm{d}t|_{error} \leq 5\%$), i_{c1} in Fig. 2*e* is approximately the same as i_{c2} in Fig. 2*j*.

Table 1 System parameters of HAPF and APF single-phase models

System parameters	Physical values
L_{c1}, L_{c2}	6 mH
R_{c1}, R_{c2}	$\simeq 0\ \Omega$
C_{c1}	70 μF
E_1, E_2	20 V (dc)

The experimental current i_{c1} and i_{c2} for their single-phase models at different switching on interval ($t = t_{on}$) are shown in Fig. 3, in which the experimental results are consistent with the simulation results as shown in Fig. 2. When $t_{on} > 1000$ μs, the slope of i_{c1} as shown in Fig. 3*a* is non-linear compared with that of i_{c2} as shown in Fig. 3*e*. Even when $t_{on} = 1000$ and 500 μs satisfy the quasi-linear limit ($T_{limit} = 1000$ μs), it is obvious that Figs. 3*b* and 3*c* contain current slope errors (35.1%, 13.4%) compared with that of APF as in Figs. 3*f* and *g*. When $t_{on} = 200$ μs, which satisfies the linear limit ($T_{linear} = 200$ μs), the current slope error decreases to 4.6% (within the linear region definition), i_{c1} in Fig. 3*d* is approximately the same as i_{c2} in Fig. 3*h*.

Since the load voltage is treated as a constant value in the analysis, its inconstant effect to the HAPF non-linearity analysis can be neglected. From Figs. 2 and 3, APF always obtains a linear current slope, whereas HAPF can obtain a non-linear current slope due to its inherent non-linear characteristic. The single-phase simulation and experimental results verified the hysteresis linearisation study of HAPF compared with that of linear APF.

3.2 Summary for determining quasi-linear limit T_{limit} and linear limit T_{linear}

In summary, the quasi-linear limit T_{limit}, linear limit T_{linear} and their corresponding hysteresis bands (H_{limit}, H_{linear}) for the HAPF can be determined in the following steps:

1. Input system parameters L_{c1} and C_{c1}, by setting $A = \cos \omega_r t = 0$, T_{limit} is the minimum value among all t values when $A = 0$ (excluding $t = 0$), where $\omega_r = \left(1/\sqrt{L_{c1}C_{c1}}\right)$. H_{limit} can then be obtained by (14).
2. Finding T_{linear} value by setting $|(\mathrm{d}i_{cx})/\mathrm{d}t|_{error} = |1 - \cos \omega_r t| = \varepsilon\%$ (11), ε is set to 5% in this study (Appendix 8.2). H_{linear} can then be obtained by (14).

4 HAPF linearisation study verification under three-phase four-wire power quality compensator application

The previous linearisation analyses and verifications are based on constant reference inverter current i_{cx}^{*} assumption (Appendix 8.2), which yields a fixed switching frequency as verified by (14) and illustrated in Fig. 4*a*. However, i_{cx}^{*} is not a constant value and unpredictable in practical three-phase four-wire power quality compensator application, thus the switching frequency of the practical HAPF system under a fixed hysteresis band value is not fixed as verified by (13) and illustrated in Fig. 4*b*. From Fig. 4*b*, when the slope of the inverter current i_{cx} keeps the same as Fig. 4*a*, it is obvious that t_{on1}, $t_{on2} > T_{linear}$ and t_{off1}, $t_{off2} < T_{linear}$ due to the variation of reference inverter current i_{cx}^{*}. In addition, when the slope of i_{cx} is the same polarity as the reference i_{cx}^{*}, t_{on1}, $t_{on2} > T_{linear}$ and vice versa. Owing to H_{linear} is set

doi: 10.1049/iet-pel.2011.0300

under a small slope error of $\varepsilon = 5\%$ in this study, it can also be treated as the linear hysteresis band limit during practical case.

In practical three-phase four-wire power quality compensator application, by setting the hysteresis band H significantly smaller than the quasi-linear limit H_{limit} or linear limit H_{linear}, it is

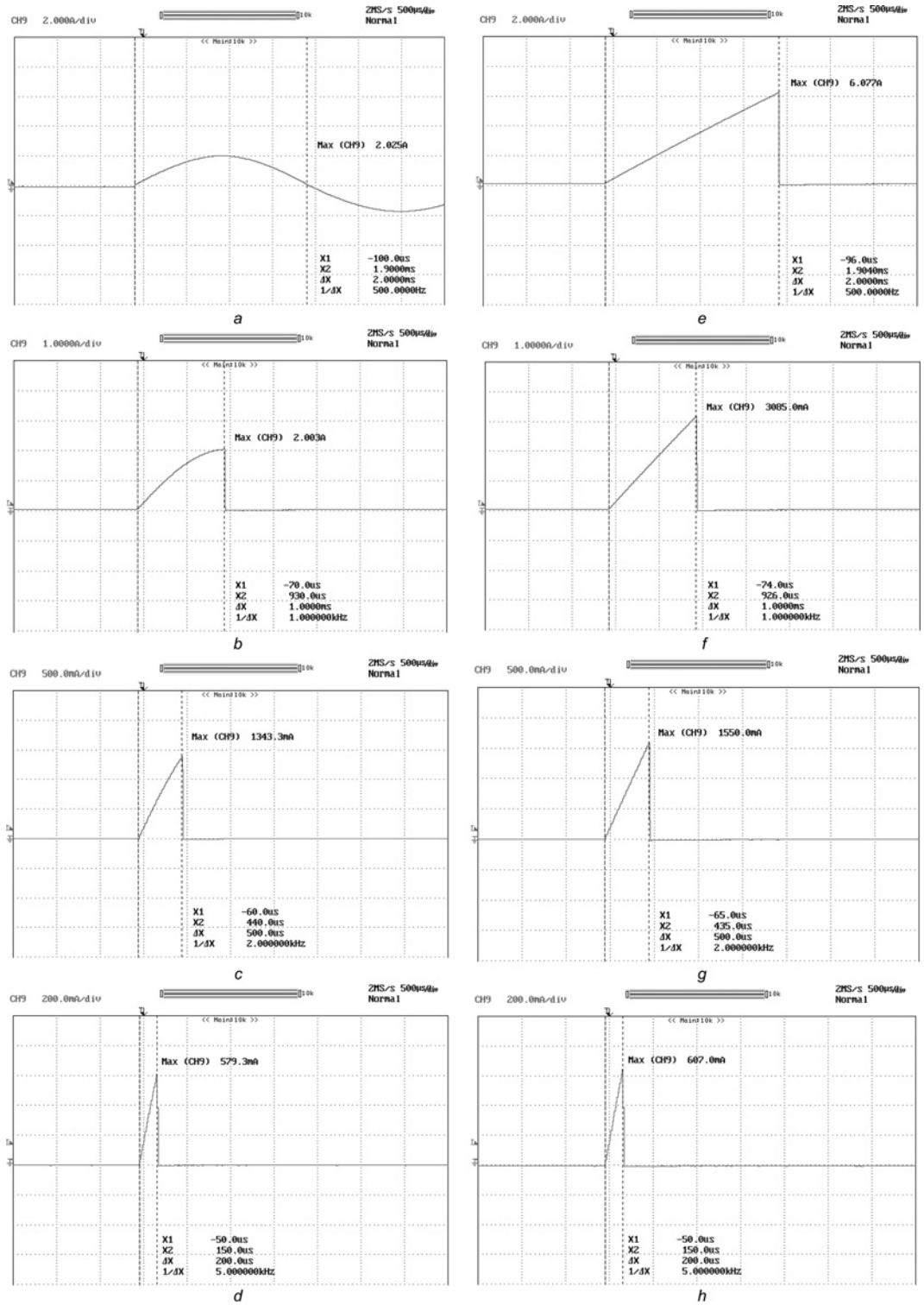

Fig. 3 *Experimental i_{c1} of HAPF and i_{c2} of APF single-phase model at different t_{on} interval and E_1, $E_2 = 20$ V*

HAPF:
a $t_{\text{on}} = 2000$ μs (non-linear)
b $t_{\text{on}} = 1000$ μs (quasi-linear)
c $t_{\text{on}} = 500$ μs (quasi-linear)
d $t_{\text{on}} = 200$ μs (linear)
APF:
e $t_{\text{on}} = 2000$ μs (linear)
f $t_{\text{on}} = 1000$ μs (linear)
g $t_{\text{on}} = 500$ μs (linear)
h $t_{\text{on}} = 200$ μs (linear)

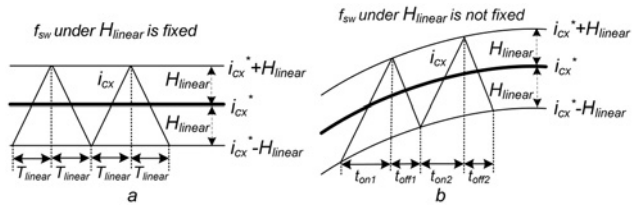

Fig. 4 *Hysteresis PWM control under H_{linear} based on*
a Previous constant i_{cx}^* assumption
b Inconstant i_{cx}^* consideration

Table 2 HAPF simulated and experimental system parameters for power quality compensation

System parameters	Physical values
v_x ($x = a, b, c$), f	55 V_{rms}, 50 Hz
L_s	0.5 mH
L_{c1}, C_{c1}, R_{c1}	6 mH, 70 μF, ≃0 Ω
C_{dc1}	5 mF
V_{dc1U}, V_{dc1L}	30 V
L_L, C_L, R_L	30 mH, 202 μF, 25 Ω

possible to keep the HAPF operates in quasi-linear region or linear region.

4.1 Determination of final sampling time T_{final} and hysteresis band H_{final}

The final sampling time T_{final} and hysteresis band H_{final} for the HAPF can be determined in the following steps:

1. For the fastest sampling time by AD converter is $T_{fastest}$, the final sampling time T_{final} can be chosen as $T_{fastest} \leq T_{final} \leq T_{linear}$.
2. For the switching frequency limitation of the switching devices is $f_{swlimit(SD)}$, the hysteresis band $H_{swlimit(SD)}$ based on $f_{swlimit(SD)}$ can be obtained through (14). Then the final hysteresis band can be chosen as $H_{swlimit(SD)} \leq H_{final} \leq H_{linear}$ in order to obtain a linear hysteresis control for the HAPF.

In the following, the HAPF linearisation study under three-phase four-wire power quality compensator application as shown in Fig. 1*a* will be investigated by both simulations and experiments. In order to simplify the verification in this part, the dc link is supported by external dc voltage source and the simulated and experimental three-phase loadings are approximately balanced. Simulation studies were carried out by using PSCAD/EMTDC. In order to verify the simulation results, a three-phase four-wire centre-split HAPF experimental prototype is also implemented in the laboratory. The control system of the prototype is a digital signal processor (DSP) TMS320F2407 and the sampling time is chosen as 50 μs (20 kHz). Moreover, the Mitsubishi IGBT intelligent power modules PM300DSA060 are employed as the switching devices for the inverter. The switching frequency limitation of the switching devices $f_{swlimit(SD)}$ is 20 kHz and the corresponding $H_{swlimit(SD)} = 0.0625$ A. Table 2 lists the HAPF simulated and experimental system parameters for power quality compensation. From Table 2, the quasi-linear limit and linear limit for HAPF can be calculated as $T_{limit} = 1000$ μs ($H_{limit} = 1.25$ A) and $T_{linear} = 200$ μs ($H_{linear} = 0.25$ A), respectively.

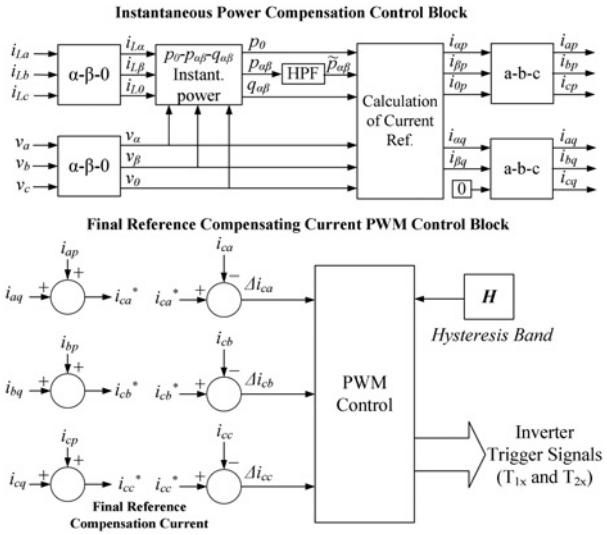

Fig. 5 *Control block diagram for the three-phase four-wire centre-split HAPF*

Fig. 5 shows the control block diagram for the three-phase four-wire HAPF, in which it consists of two main control blocks: instantaneous power compensation control block and final reference compensating current PWM control block. From Fig. 5, the reference compensating active and reactive currents for the HAPF (i_{xp}, i_{xq}, the subscript $x = a$, b, c for three-phases) are determined based on the three-phase instantaneous pq theory [17]. The final reference compensating current i_{cx}^* can be obtained by summing up the i_{xp} and i_{xq}, which can compensate both the reactive, harmonic and neutral currents. Then the compensating current error Δi_{cx} together with hysteresis band H will be sent to the current PWM control part for generating PWM trigger signals to the IGBTs. In the following, representative simulation and experimental results are included to illustrate and verify the HAPF inverter current slope linearisation study under three-phase power quality compensator application.

4.2 Simulation results

Fig. 6*a* shows the simulated reference inverter current i_{cx}^*, and Figs. 6*b*–*d* depict the simulated inverter current i_{cx} when the HAPF is operating at non-linear region, quasi-linear region and linear region. Table 3 summarises their corresponding simulation results before and after compensation.

1. *Non-linear region:* As $T_{limit} = 1000$ μs ($H_{limit} = 1.25$ A), the hysteresis band $H = 1.25$ A will keep the HAPF operating at non-linear region. The polarity of the inverter current slope has interchanging before i_{cx} touches the band H at some instances, which can be verified by Fig. 6*b*. Table 3 illustrates that the HAPF can compensate the system displacement power factor (DPF) from 0.83 into unity. However, the non-linear slope of i_{cx} deteriorates the compensation results ($THD_{i_{sx}} = 31.2\%$, $THD_{V_x} = 7.2\%$, system neutral current $i_{sn} = 1.40$ A_{rms}) by generating unexpected trigger signals to the switching devices. Moreover, both compensated $THD_{i_{sx}}$ and THD_{V_x} do not satisfy the international standards [18, 19]. From Table 3, the system average operating switching frequency is 0.6 kHz.

doi: 10.1049/iet-pel.2011.0300

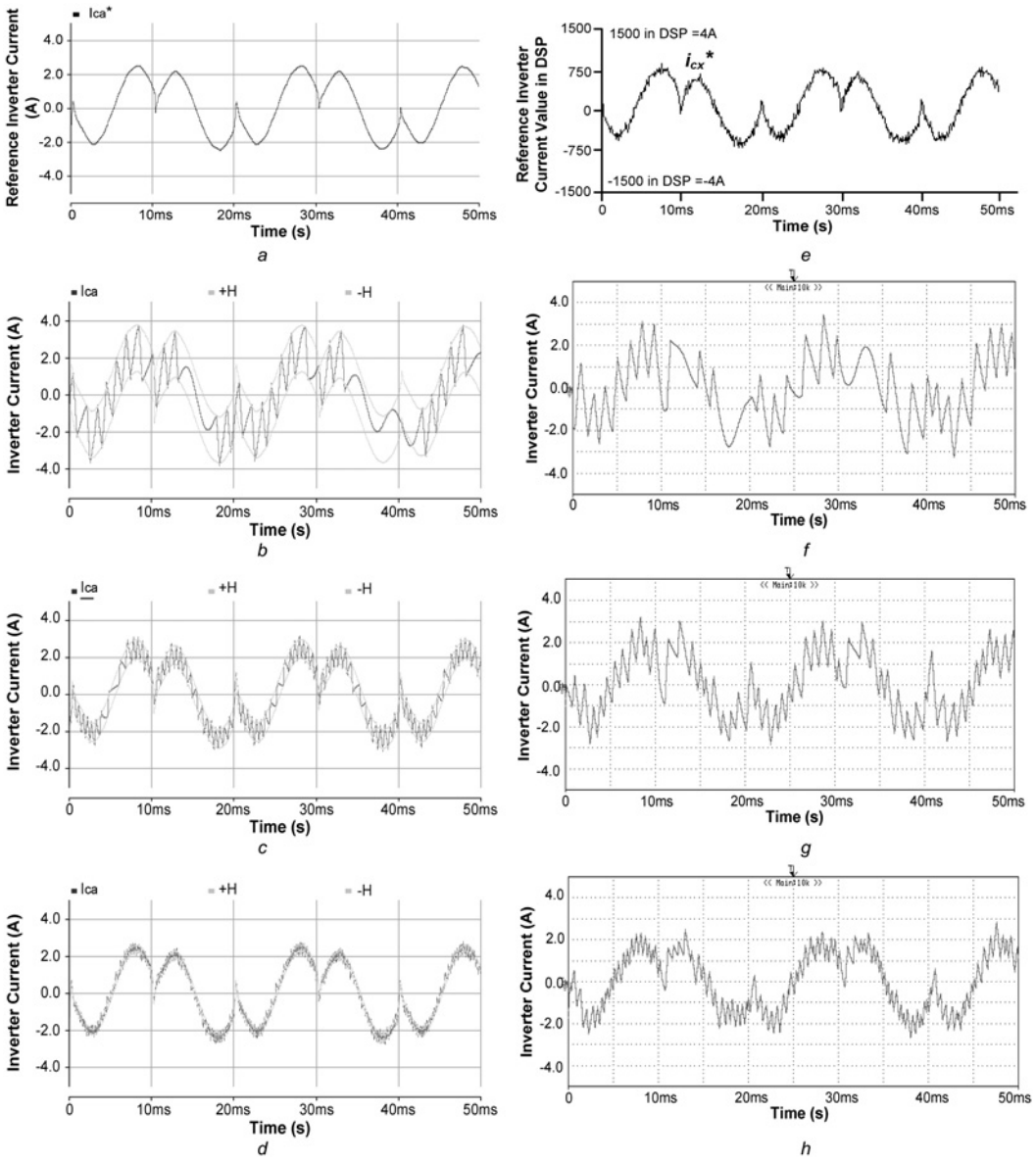

Fig. 6 *Simulated and experimental i^*_{cx} and i_{cx} for HAPF at different operation regions*

Simulated results:
a Reference inverter current i^*_{cx}
b Non-linear region ($H = 1.25$ A)
c Quasi-linear region ($H = 0.50$ A)
d Linear region ($H = 0.156$ A)
Experimental results:
e Reference inverter current i^*_{cx} in DSP
f Non-linear region ($H = 1.25$ A)
g Quasi-linear region ($H = 0.50$ A)
h Linear region ($H = 0.156$ A)

2. *Quasi-linear region:* Setting the band $H = 0.50$ A can keep the HAPF operating at quasi-linear region. The polarity of the inverter current slope changes only when i_{cx} touches the band H, as shown in Fig. 6*c*. The system DPF has been compensated into unity and $i_{sn} = 0.68\ A_{rms}$. When HAPF is operating at quasi-linear region, the current slope error is significant, which affects the system performances. This phenomenon can be verified by showing compensated $THD_{i_{sx}} = 17.3\%$ and $THD_{V_x} = 6.6\%$ as shown in Table 3, in which both of them do not satisfy the international standards [18, 19]. From Table 3, the system average operating switching frequency is 1.7 kHz.

3. *Linear region:* As $T_{linear} = 200\ \mu s$ ($H_{linear} = 0.25$ A) and $H_{swlimit(SD)} = 0.0625$ A, the hysteresis band $H = 0.156$ A can satisfy both the linear limit and the switching frequency limitation of the switching devices. This band value can keep the HAPF operating at linear region as verified by Fig. 6*d*. Table 3 illustrates that $H = 0.156$ A yields the best compensation performances among the three operation regions. The system current, system neutral current, system DPF after compensation becomes sinusoidal ($THD_{i_{S_x}} = 6.2\%$), less ($0.32\ A_{rms}$), unity and $THD_{V_x} = 2.8\%$, in which all the results satisfy the international standards [18, 19]. From Table 3, the system

Table 3 Simulation results for hysteresis PWM controlled HAPF before and after compensation at different operation regions

	HAPF with V_{dc1U}, $V_{dc1L} = 30$ V, $C_{c1} = 70$ μF, $L_{c1} = 6$ mH			
	Before compensation	After compensation		
		(a) $H = 1.25$ A (non-linear)	(b) $H = 0.50$ A (quasi-linear)	(c) $H = 0.156$ A (linear)
system current i_{sx} (A_{rms})	2.67	2.36	2.17	2.12
system DPF	0.83	1.00	1.00	1.00
total harmonics distortion of system current THD_{isx} (%)	28.0	31.2	17.3	6.2
total harmonics distortion of load voltage THD_{Vx} (%)	2.1	7.2	6.6	2.8
system neutral current i_{sn} (A_{rms})	2.18	1.40	0.68	0.32
average operating switching frequency f_{sw} (Hz)	–	0.6 k	1.7 k	5.1 k

average operating switching frequency is 5.1 kHz. When H is further decreased, the HAPF can obtain better compensation results as the slope error can be reduced.

4.3 Experimental results

Fig. 6*e* shows the experimental reference inverter current i^*_{cx} in DSP, and Figs. 6*f–h* depict the experimental inverter current i_{cx} when the HAPF is operating at non-linear region, quasi-linear region and linear region. Table 4 summarises their experimental results before and after compensation.

1. *Non-linear region:* As $T_{limit} = 1000$ μs ($H_{limit} = 1.25$ A), the hysteresis band $H = 1.25$ A will keep the HAPF operating at non-linear region. The polarity of the inverter current slope has interchanging before i_{cx} touches the band H at some instances, as shown in Fig. 6*f*. Table 4 illustrates that the HAPF can compensate the system DPF close to unity. However, the non-linear slope of i_{cx} deteriorates the compensation results ($THD_{i_{sx}} = 27.3\%$, $THD_{V_x} = 5.6\%$ for the worst phase, $i_{sn} = 1.46\ A_{rms}$) by generating unexpected trigger signals to the switching devices. Moreover, both compensated $THD_{i_{sx}}$ and THD_{V_x} do not satisfy the international standards [18, 19]. From Table 4, the system average operating switching frequency is 0.5 kHz.

2. *Quasi-linear region*: Setting the band $H = 0.50$ A can keep the HAPF operating at quasi-linear region. The polarity of the inverter current slope changes only when i_{cx} touches the band H, as shown in Fig. 6*g*. The system DPF has been compensated close to unity. When HAPF is operating at quasi-linear region, the current slope error is significant, which affects the operating performances ($THD_{i_{sx}} = 16.4\%$ and $THD_{V_x} = 4.3\%$ for the worst phase, $i_{sn} = 0.98\ A_{rms}$) as shown in Table 4, and the compensated $THD_{i_{sx}}$ does not satisfy the international standards [18, 19]. From Table 4, the system average operating switching frequency is 1.1 kHz.

3. *Linear region:* As $T_{linear} = 200$ μs ($H_{linear} = 0.25$ A) and $H_{swlimit(SD)} = 0.0625$ A, the hysteresis band $H = 0.156$ A can satisfy both the linear limit and the switching frequency limitation of the switching devices. This band value can keep the HAPF operating at linear region as verified by

Table 4 Experimental results for hysteresis PWM controlled HAPF before and after compensation at different operation regions

		HAPF with V_{dc1U}, $V_{dc1L} = 30$ V, $C_{c1} = 70$ μF, $L_{c1} = 6$ mH			
		Before compensation	After compensation		
			(a) $H = 1.25$ A (non-linear)	(b) $H = 0.50$ A (quasi-linear)	(c) $H = 0.156$ A (linear)
system current i_{sx} (A_{rms})	*A*	2.42	2.21	2.13	2.10
	B	2.42	2.20	2.14	2.11
	C	2.35	2.07	1.96	1.94
system DPF	*A*	0.86	1.00	1.00	1.00
	B	0.89	1.00	1.00	1.00
	C	0.86	1.00	1.00	1.00
total harmonics distortion of system current THD_{isx} (%)	*A*	23.2	27.3	16.1	9.5
	B	22.4	25.9	16.4	9.2
	C	23.4	26.2	16.0	9.8
total harmonics distortion of load voltage THD_{Vx} (%)	*A*	2.5	5.6	4.3	2.8
	B	2.4	5.2	4.2	3.0
	C	2.5	5.1	4.2	2.9
system neutral current i_{sn} (A_{rms})	*N*	1.57	1.46	0.98	0.64
average operating switching frequency f_{sw} (Hz)	*A*	–	0.5 k	1.1 k	3.1 k
	B				
	C				

doi: 10.1049/iet-pel.2011.0300

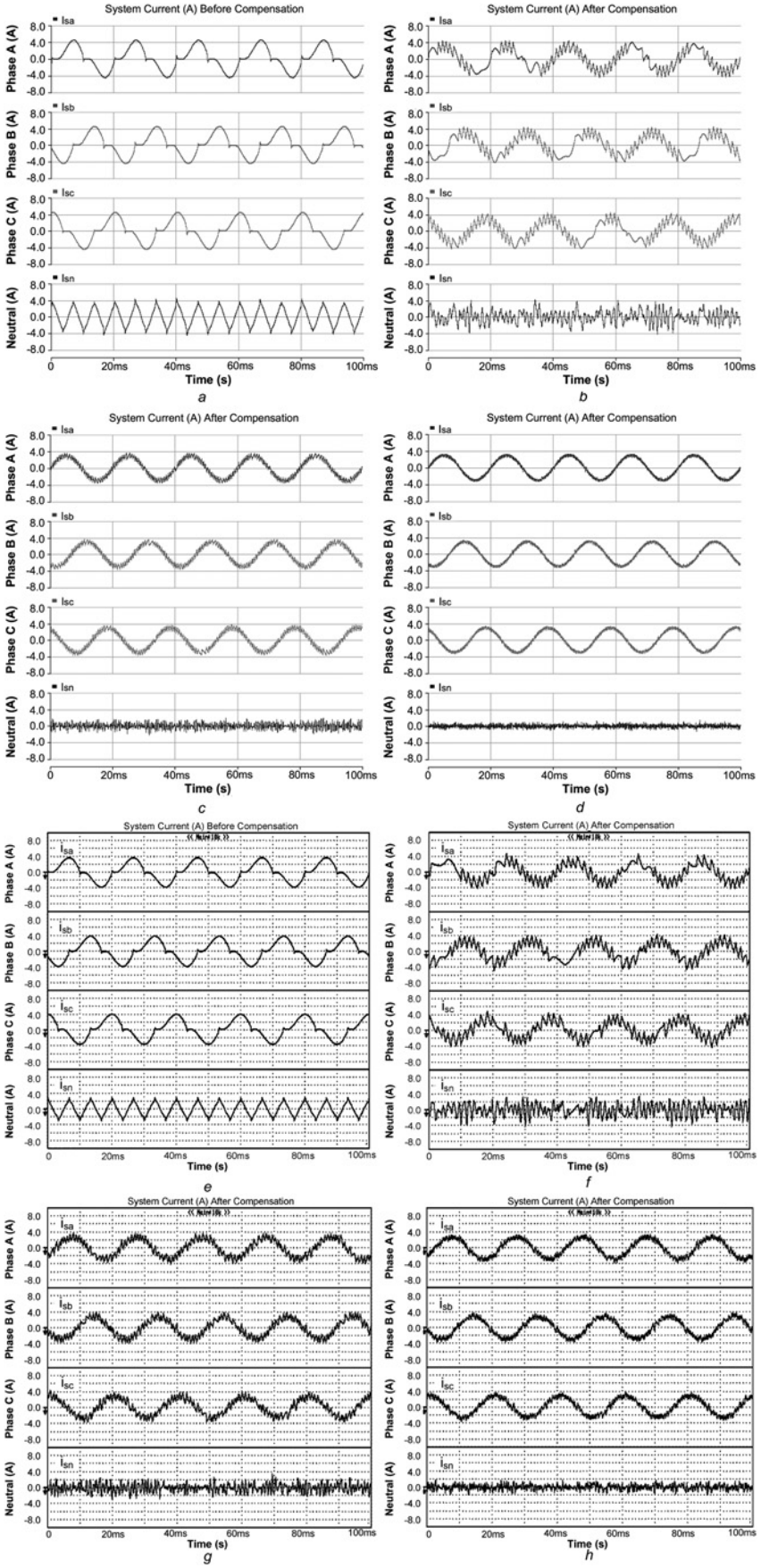

Fig. 7 *Simulated and experimental i_{sx} before and after HAPF compensation at different operation regions*

Simulated results:
a Before compensation
b Non-linear region ($H = 1.25$ A)
c Quasi-linear region ($H = 0.50$ A)
d Linear region ($H = 0.156$ A)

Experimental results:
e Before compensation
f Non-linear region ($H = 1.25$ A)
g Quasi-linear region ($H = 0.50$ A)
h Linear region ($H = 0.156$ A)

Fig. 6*h*. Table 4 illustrates that $H = 0.156$ A yields the best compensation performance among the three operation regions. The system DPF has been compensated close to unity, $\text{THD}_{i_{sx}} = 9.8\%$ and $\text{THD}_{V_x} = 3.0\%$ for the worst phase, $i_{sn} = 0.64\ A_{rms}$, in which all the compensated results satisfy the international standards [18, 19]. From Table 4, the system average operating switching frequency is 3.1 kHz.

Comparing Table 4 with Table 3, there are differences between simulation and experimental results, which are actually due to the difference of component parameters, the resolution of the transducers, the digital computation error and the noise in the experiment. Moreover, those factors will affect the HAPF compensation performances significantly in linear region operation because more precise A/D signals, computation and control for the HAPF are required. In order to improve the performances (reduce the slope error) of the HAPF experimental prototype, the hysteresis band H value can be further reduced.

The experimental results as in Figs. 6*e*–*h* and Table 4 agreed with the simulation results as in Figs. 6*a*–*d* and Table 3, which verified the hysteresis linearisation study for HAPF under three-phase four-wire power quality compensator application. In addition, the HAPF can compensate the system DPF to unity among the three operation regions. However, only when the HAPF is operating at linear operation region, the compensated $\text{THD}_{i_{sx}}$ and THD_{V_x} can satisfy the international standards [18, 19].

Figs. 7*e*–*f* depict the experimental three-phase system current i_{sx} before and after compensation, in which the results are consistent with the simulation results as shown in Figs. 7*a*–*d*. And the current harmonics and neutral current can only be significantly compensated at HAPF linear operation region. When the HAPF operates at linear region, it can obtain acceptable current quality compensation performances (Tables 3 and 4) with an average power loss of about 4.0% of the loading power consumption and a fast response time of less than 10 ms.

5 Conclusion

In this study, the characteristic and linear requirement of hysteresis PWM control for a LC-coupling HAPF are investigated and discussed. On the basis of the modeling, the non-linear phenomenon and linearisation process for the HAPF inverter current slope are studied, explored and compared with that of the linear APF. Two limits quasi-linear limit and linear limit are proposed, which separate the HAPF into non-linear, quasi-linear and linear operation regions. In order to ensure the controllability of using the conventional hysteresis control and to avoid obtaining unexpected trigger signals for the switching devices, the hysteresis band and sampling time should satisfy the linear limit requirement. Single-phase simulation and experimental results are presented to verify the hysteresis linearisation study of the HAPF and compared with that of the APF. Finally, representative simulation and experimental results of HAPF under three-phase power quality compensation system are given to prove the validity of the hysteresis linearisation study.

6 Acknowledgment

The authors thank the Science and Technology Development Fund, Macao SAR Government and Research Committee of University of Macau for their financial supports.

7 References

1 Bose, B.: 'Power electronics and variable frequency drives: technology and applications' (IEEE Press, New York, 1997)
2 Brod, D.M., Novotny, D.W.: 'Current control of VSI-PWM inverters', *IEEE Trans. Ind. Appl.*, 1985, **21**, (4), pp. 562–570
3 Bose, B.K.: 'An adaptive hysteresis-band current control technique of a voltage-fed PWM inverter for machine drive system', *IEEE Trans. Ind. Appl.*, 1990, **37**, (5), pp. 402–408
4 Kang, B.-J., Liaw, C.-M.: 'A robust hysteresis current-controlled PWM inverter for linear PMSM driven magnetic suspended positioning system', *IEEE Trans. Ind. Appl.*, 2001, **48**, (5), pp. 956–967
5 Malesani, L., Mattavelli, P., Tomasin, P.: 'High-performance hysteresis modulation technique for active filters', *IEEE Trans. Power Electron.*, 1997, **12**, (5), pp. 876–884
6 Casadei, D., Serra, G., Tani, A., Zarri, L.: 'Theoretical and experimental analysis for the RMS current ripple minimization in induction motor drives controlled by SVM technique', *IEEE Trans. Ind. Electron.*, 2004, **51**, (5), pp. 1056–1065
7 Shen, D., Lehn, P.W.: 'Fixed-frequency space-vector-modulation control for three-phase four-leg active power filters', *IEE Proc. Electr. Power Appl.*, 2002, **149**, (4), pp. 268–274
8 Zhang, R., Prasad, V.H., Boroyevich, D., Lee, F.C.: 'Three-dimensional space vector modulation for four-leg voltage-source converters', *IEEE Trans. Power Electron.*, 2002, **17**, (3), pp. 314–326
9 Zhan, C.J., Arulampalam, A., Jenkins, N.: 'Four-wire dynamic voltage restorer based on a three-dimensional voltage space vector PWM algorithm', *IEEE Trans. Power Electron.*, 2003, **18**, (4), pp. 1093–1102
10 Fujita, H., Akagi, H.: 'A practical approach to harmonic compensation in power systems – series connection of passive and active filters', *IEEE Trans. Ind. Appl.*, 1991, **27**, (6), pp. 1020–1025
11 Park, S., Sung, J.-H., Nam, K.: 'A new parallel hybrid filter configuration minimizing active filter size'. Proc. IEEE 30th Annual Power Electronics Specialists Conf., PESC 99, 1999, vol. 1, pp. 400–405
12 Peng, F.Z., Akagi, H., Nabae, A.: 'A new approach to harmonic compensation in power systems – a combined system of shunt passive and series active filters', *IEEE Trans. Ind. Appl.*, 1990, **26**, (6), pp. 983–990
13 Srianthumrong, S., Akagi, H.: 'A medium-voltage transformerless AC/DC Power conversion system consisting of a diode rectifier and a shunt hybrid filter', *IEEE Trans. Ind. Appl.*, 2003, **39**, (3), pp. 874–882
14 Tangtheerajaroonwong, W., Hatada, T., Wada, K., Akagi, H.: 'Design and performance of a transformerless shunt hybrid filter integrated into a three-phase diode rectifier', *IEEE Trans. Power Electron.*, 2007, **22**, (5), pp. 1882–1889
15 Rahmani, S., Hamadi, A., Mendalek, N., Al-Haddad, K.: 'A new control technique for three-phase shunt hybrid power filter', *IEEE Trans. Ind. Electron.*, 2009, **56**, (8), pp. 2904–2915
16 Inzunza, R., Akagi, H.: 'A 6.6-kV transformerless shunt hybrid active filter for installation on a power distribution system', *IEEE Trans. Power Electron.*, 2005, **20**, (4), pp. 893–900
17 Akagi, H., Ogasawara, S., Hyosung, K.: 'The theory of instantaneous power in three-phase four-wire systems: a comprehensive approach'. Conf. Rec. IEEE – 34th IAS Annual Meeting, 1999, vol. 1, pp. 431–439
18 IEEE Standard 519-1992: 'IEEE recommended practices and requirements for harmonic control in electrical power systems', 1992
19 IEC Standard 61000-3-2: 'Electromagnetic compatibility (EMC), part 3: limits, section 2: limits for harmonics current emissions (equipment input current ≤16A per phase)', 1997

8 Appendix

8.1 Non-linearity of HAPF inverter current slope

The definitions and diagrams for the HAPF operating in (i) non-linear region, (ii) quasi-linear region and (iii) linear region under hysteresis control are given below:

1. *Non-linear region:* The slope of the HAPF inverter current i_{cx} is defined as 'non-linear' if its slope polarity has interchanged from positive to negative or vice versa before i_{cx} touches the top or bottom hysteresis band H (within each switching interval), as shown in Fig. 8*a*. i_{cx}^* is the reference inverter current.

doi: 10.1049/iet-pel.2011.0300

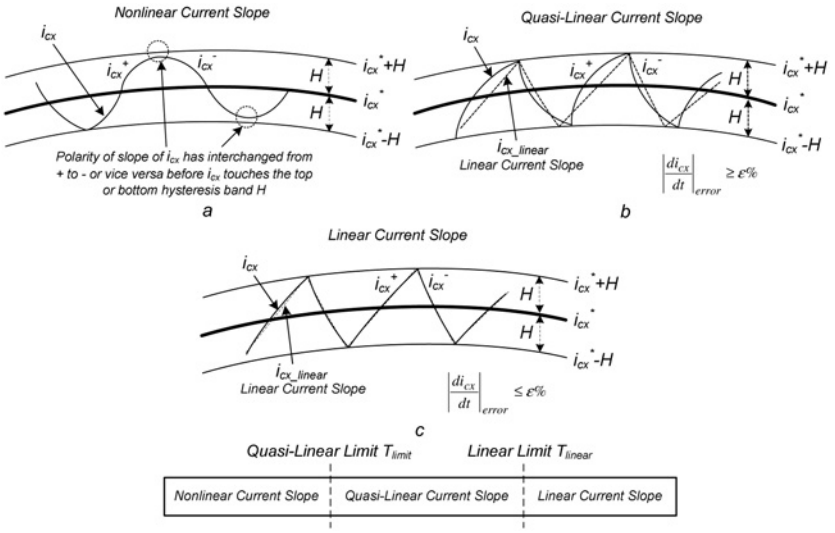

Fig. 8 *Slope of the HAPF inverter current i_{cx} under hysteresis PWM control*

a Non-linear region
b Quasi-linear region
c Linear region

2. *Quasi-linear region:* The slope of the HAPF inverter current i_{cx} is defined as 'quasi-linear' if its slope polarity changes only when i_{cx} touches the top or bottom hysteresis band H. Within each switching on or off interval, the absolute percentage error of its current slope compared with a linear one is larger than $\varepsilon\%$ ($|(\mathrm{d}i_{cx})/\mathrm{d}t|_{error} > \varepsilon\%$), as shown in Fig. 8*b*.
3. *Linear region:* The slope of the HAPF inverter current i_{cx} can be treated as 'linear' if its slope polarity changes only when i_{cx} touches the top or bottom hysteresis band H. Within each switching on or off interval, the absolute percentage error of its current slope compared with a linear one is less than or equal to $\varepsilon\%$ ($|(\mathrm{d}i_{cx})/\mathrm{d}t|_{error} \leq \varepsilon\%$), as shown in Fig. 8*c*.

When the coupling part internal resistance is small, $R_{c1} \simeq 0$, the HAPF will be an underdamped system. Combining (4) and (6), the complete response of coupling capacitor voltage $v_{Cc1x(t)}$ can be derived. Then the HAPF inverter current i_{cx} can be deduced by taking derivative of $v_{Cc1x(t)}$ via (6). After that, taking derivative of i_{cx} will yield the rate of change of inverter current ($\mathrm{d}i_{cx}/\mathrm{d}t$). As the initial condition of i_{cx} will not affect the non-linear nature of the inverter current slope, it can be simply treated as zero. Substitute this initial condition into ($\mathrm{d}i_{cx}/\mathrm{d}t$) during each switching interval, this yields

$$\frac{\mathrm{d}i_{cx}(t)}{\mathrm{d}t} = -\omega_r^2 C_{c1} B_1 A \tag{9}$$

where t represents each switching on or off interval ($t = t_{on}$ or t_{off}), $\omega_r = \left(1/\sqrt{L_{c1}C_{c1}}\right)$, B_1 is a real number and kept constant at each switching interval, and $A = \cos\omega_r t$. In order to prevent the current slope from being non-linear, the polarity of (9) should be kept unchanged within each switching interval as shown in Fig. 8. However, due to the non-linear term $A = \cos\omega_r t$, its polarity may have interchanging within each switching on or off interval. In addition, the non-linear term is mainly affected by the coupling part (C_{c1}, L_{c1}) and the switching frequency f_{sw}. As the coupling part is designed basing on the reactive power consumption and the dominant harmonic current of the loading, the effect of changing the coupling part values will not be studied. As a result, only the effect of changing the switching frequency will be investigated in this paper. In the following, the quasi-linear limit T_{limit} and linear limit T_{linear} that divides the HAPF into non-linear, quasi-linear and linear regions will be determined based on a constant reference inverter current i_{cx}^* ($\mathrm{d}i_{cx}^*/(\mathrm{d}t) = 0$) assumption. Then the quasi-linear limit H_{limit} and linear limit H_{linear} for the hysteresis band can be obtained correspondingly.

8.2 Quasi-linear limit T_{limit} and linear limit T_{linear} for HAPF inverter current slope

From Fig. 8, the quasi-linear limit T_{limit} and linear limit T_{linear} will be deduced based on one switching interval (t_{on} or t_{off}) analysis. As the hysteresis control method yields asymmetric switching on and off intervals during operation, by choosing the switching frequency $f_{sw} = 1/(t_{on} + t_{off}) \geq 1/2T_{limit}$ or $f_{sw} \geq 1/2T_{linear}$, it is possible that either switching on or off interval cannot satisfy the limit T_{limit} or T_{linear}. As a result, in order to ensure that each switching interval satisfies the limit, the switching frequency should be chosen as $f_{sw} \geq 1/T_{limit}$ or $f_{sw} \geq 1/T_{linear}$. As a result, once the limits are determined, the inverse of these limits are treated as the quasi-linear limit and linear limit for the switching frequency f_{sw}.

Fig. 9*a* illustrates the graphs of non-linear term A at different time t and $R_{c1} \simeq 0$. From Fig. 9*a*, in order to prevent the HAPF current slope from being non-linear, the switching frequency f_{sw} and sampling time T can be chosen as

$$f_{sw} \geq \frac{1}{T_{limit}}, \quad T \leq T_{limit} \quad \text{and} \quad T \leq \frac{1}{f_{sw}} \tag{10}$$

where T_{limit} is the quasi-linear limit for each switching on or off interval.

From (9), the absolute error of the HAPF inverter current slope ($|(\mathrm{d}i_{cx})/\mathrm{d}t|_{error}$) compared with a linear one can be

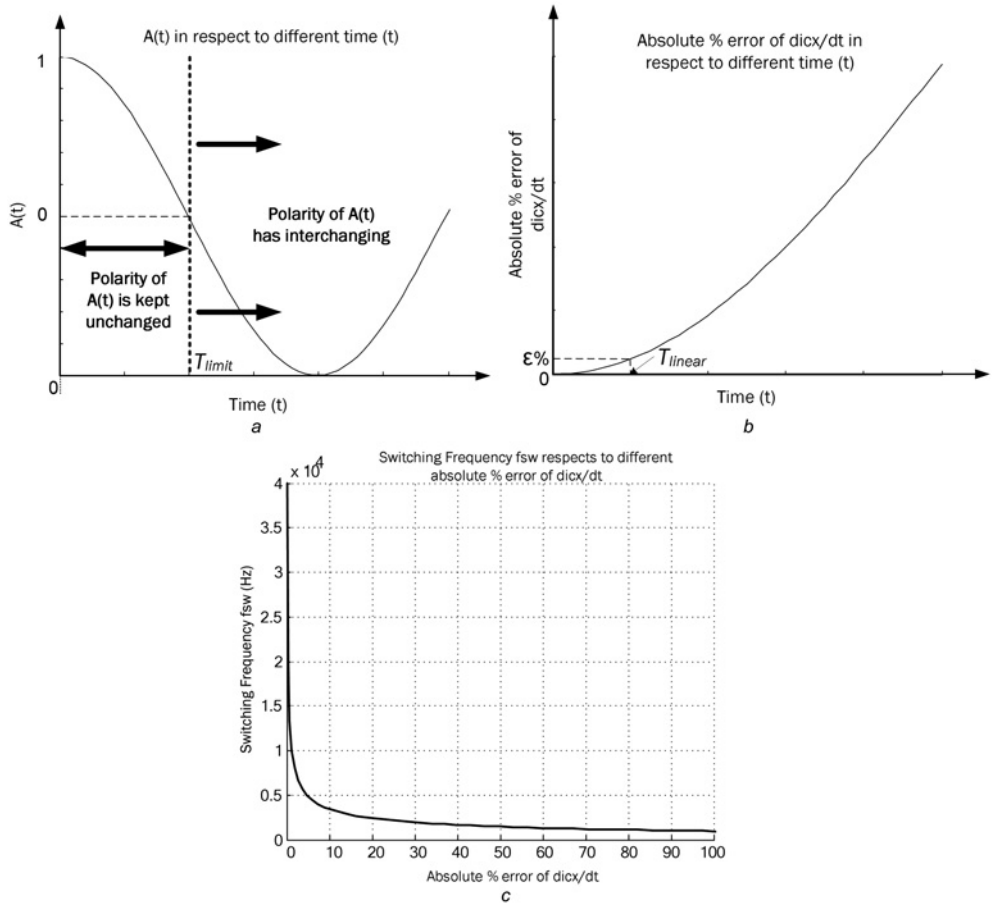

Fig. 9 *Graphs of $A = \cos\omega_r t$, $|(di_{cx})/dt|_{error}$ and f_{sw} against $|(di_{cx})/dt|_{error}$*

a $A = \cos\omega_r t$ at different time t and $R_{c1} \simeq 0$
b $|(\mathrm{d}i_{cx})/\mathrm{d}t|_{error}$ at different time t and $R_{c1} \simeq 0$
c f_{sw} against $|(\mathrm{d}i_{cx})/\mathrm{d}t|_{error}$

expressed as

$$\left|\frac{\mathrm{d}i_{cx}}{\mathrm{d}t}\right|_{error} = |1 - \cos\omega_r t| \tag{11}$$

From Fig. 8*c*, once $(|(\mathrm{d}i_{cx})/\mathrm{d}t|_{error} \leq \varepsilon\%)$ is satisfied, the inverter current slope can be approximately treated as linear. From Fig. 9*b*, if each switching interval is less than T_{linear}, it can satisfy the HAPF linear region definition $(|(\mathrm{d}i_{cx})/\mathrm{d}t|_{error} \leq \varepsilon\%)$. In order to obtain a linear inverter current slope, the switching frequency f_{sw} and sampling time T can be chosen as

$$f_{sw} \geq \frac{1}{T_{linear}}, \quad T \leq T_{linear} \quad \text{and} \quad T \leq \frac{1}{f_{sw}} \tag{12}$$

where T_{linear} is the linear limit for each switching on or off interval.

From Fig. 8, if the current slope error limit ε is set to be large, the HAPF will result in low switching frequency and loss, but with a large operational error. When ε is set close to zero, it is impractical due to a high switching frequency requirement for the switching devices. Fig. 9*c* shows the switching frequency f_{sw} requirement in respect to different absolute percentage error $(|(\mathrm{d}i_{cx})/\mathrm{d}t|_{error})$of the current slope. From Fig. 9*c*, when $(|(\mathrm{d}i_{cx})/\mathrm{d}t|_{error})$ is desired to be decreased a little bit more from 5%, the switching frequency requirement will exponentially increase a lot. In this study, ε is set at 5% because its corresponding switching frequency is within limitation of the switching devices. Moreover, the HAPF compensation performances under $\varepsilon = 5\%$ consideration are acceptable as verified by the simulation and experimental results in Section 4.

8.3 Relationship among hysteresis band H, switching frequency f_{sw} and dc-link voltage V_{dc1} of linearised HAPF

Fig. 10 shows the hysteresis current-controlled PWM for HAPF: Fig. 10*a* switching scheme block diagram for one phase and Fig. 10*b* current and voltage waveforms before and after linearisation. From Fig. 10, the relationship among the switching frequency f_{sw}, hysteresis band H, dc-link voltage V_{dc1} under HAPF linear region can be derived. After simplification, the hysteresis band H value under a fixed switching frequency f_{sw} can be approximately expressed as

$$H \simeq \frac{V_{dc1}}{8L_{c1}f_{sw}}\left[1 - \frac{4L_{c1}^2}{V_{dc1}^2}m^2\right] \tag{13}$$

where $m = (\mathrm{d}i_{cx}^*/dt)$ is the slope of the reference inverter current i_{cx}^*.

As the reference inverter current is assumed to be a constant value during the previous linearisation analysis,

doi: 10.1049/iet-pel.2011.0300

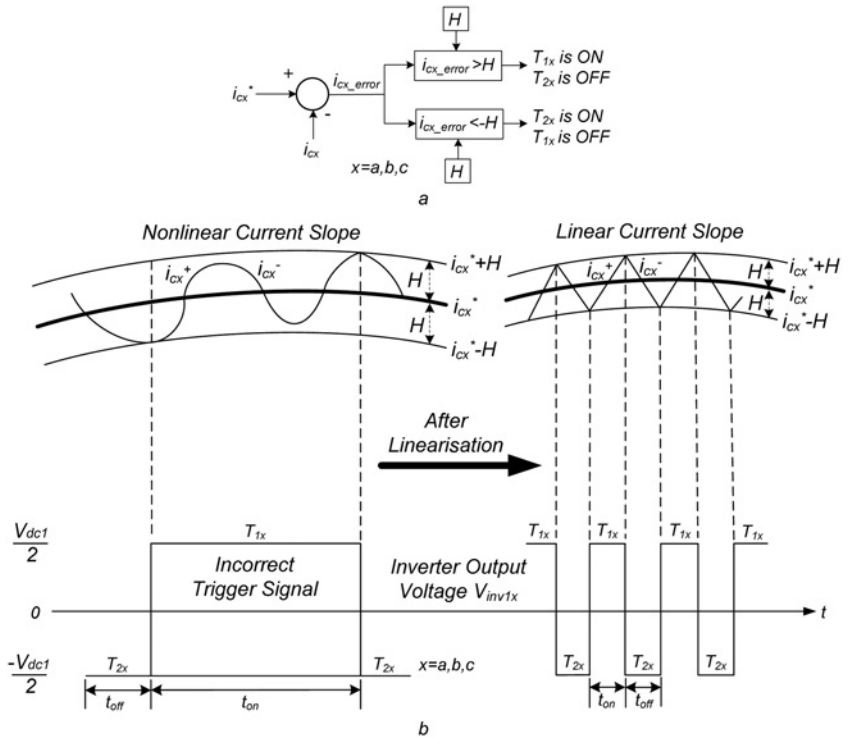

Fig. 10 *Hysteresis current-controlled PWM for HAPF*

a Switching scheme block diagram for one phase
b Current and voltage waveforms before and after linearisation

(13) becomes

$$H = \frac{V_{dc1}}{8L_{c1}f_{sw}} \tag{14}$$

Substituting $f_{sw} = 1/T_{limit}$ or $1/T_{linear}$ into (14), this yields the quasi-linear limit H_{limit} or linear limit H_{linear} for the hysteresis band. Under constant reference inverter current i_{cx}^* assumption, the system operating switching frequency under H_{limit} or H_{linear} will be fixed. When i_{cx}^* is not a constant value, (14) will yield the HAPF maximum operating switching frequency under a fixed hysteresis band.